Stanford Exploration Project, Report 103, April 28, 2000, pages 1–19

Tau tomography with steering filters: 2-D field data example

Robert G. Clapp and Biondo L. Biondi[1]

ABSTRACT

Common reflection point (CRP) gathers are usually parameterized in terms of offset. For tomography, a more convenient parameterization is in terms of reflection angle. Reflection angle CRP gathers can be constructed using wave equation migration. By performing tomography in vertical travel-time (tau), focusing velocity, rather than some combination of focusing and mapping velocity, can be estimated. By using anisotropic preconditioning oriented along bedding planes, the solution can be guided towards a geologically reasonable model. The benefits of the tomography method are shown on a 2-D line from a 3-D marine dataset.

INTRODUCTION

Tomography is inherently non-linear, therefore a standard technique is to linearize the problem by assuming a stationary ray field (Stork and Clayton, 1991). Unfortunately, we must still deal with the coupled relationship between reflector position and velocity (Al-Chalabi, 1997; Tieman, 1995). As a result, the back projection operator must attempt to handle both repositioning of the reflector *and* updating the velocity model (van Trier, 1990) . The resulting back projection operator is sensitive to our current guess at velocity and reflector position. In vertical traveltime space, reflector movement is significantly less. Biondi et al. (1998b) showed that by reformulating the problem in this space, complex velocity functions could be obtained more quickly and are better resolved.

In ray-based migration velocity analysis, Kirchhoff migration is normally used to construct CRP gathers and residual moveout. Unfortunately, conventional implementation of Kirchhoff methods have trouble handling complex wave behavior. Wave equation methods are an attractive alternative to Kirchhoff. Clayton and Stolt (1981) and later Prucha et al. (1999) showed that wave equation methods can form CRP gathers in terms of reflection angle.

Tomography problems are also often under-determined. By adding an additional model regularization term to our objective function (Toldi, 1985) we can stabilize the inversion. In theory, this regularization term should be the inverse model covariance matrix (Tarantola, 1987). Clapp et al. (1998a) constructed a series of small plane wave annihilators, called steer-

[1]**email:** bob@sep.stanford.edu,biondo@sep.stanford.edu

ing filters, using *a priori* information to produce changes to our velocity model that were more geologically reasonable.

In this paper we show how to apply steering filters to smooth the slowness, rather than the change in slowness. We use wave equation CRP gathers as the basis for ray based tomography. We apply the technique on a 2-D line taken from a 3-D marine dataset from the North Sea. We show that we can obtain a velocity model that improves the focusing of the data while being geologically reasonable.

REVIEW

Following the methodology of Clapp and Biondi (1999) we will begin by considering a regularized tomography problem. We will linearize around an initial slowness estimate and find a linear operator in the vertical traveltime domain $\mathbf{T}$ between our change in slowness $\Delta\mathbf{s}$ and our change in traveltimes $\Delta\mathbf{t}$. We will write a set of fitting goals,

$$\begin{aligned} \Delta\mathbf{t} &\approx \mathbf{T}\Delta\mathbf{s} \\ \mathbf{0} &\approx \epsilon\mathbf{A}\Delta\mathbf{s}, \end{aligned} \tag{1}$$

where $\mathbf{A}$ is our steering filter operator and ϵ is a Lagrange multiplier. However, these fitting goals don't accurately describe what we really want. Our steering filters are based on our desired slowness rather than change of slowness. With this fact in mind, we can rewrite our second fitting goal as:

$$\mathbf{0} \approx \mathbf{A}(\mathbf{s_0} + \Delta\mathbf{s}) \tag{2}$$

$$-\epsilon\mathbf{A}\mathbf{s_0} \approx \epsilon\mathbf{A}\Delta\mathbf{s}. \tag{3}$$

Our second fitting goal can not be strictly defined as regularization but we can do a preconditioning substitution (Fomel et al., 1997):

$$\begin{aligned} \Delta\mathbf{t} &\approx \mathbf{T}\mathbf{A}^{-1}\mathbf{p} \\ -\epsilon\mathbf{A}\mathbf{s_0} &\approx \epsilon\mathbf{I}\mathbf{p}. \end{aligned} \tag{4}$$

Wave equation angle gathers

When doing velocity analysis, general practice is to measure moveout from a relatively sparse set of CRP gathers. Kirchhoff depth migration is the preferred construction method because it can produce the sparse set of CRP gathers without needing to image the entire volume. In addition, if our Green's function table is constructed correctly, Kirchhoff methods do not suffer from the velocity approximations needed by frequency domain methods. Kirchhoff methods also have some deficiencies. The most glaring weakness of Kirchhoff methods is the difficulty in constructing the Green's function table. To construct an accurate Green's

function table we must account for, and weight correctly, the multiple arrivals that occur in complex geology. Calculating and accounting for multiple arrivals adds significantly to both coding complexity and memory requirements. As a result, a single arrival is often all that is used. Eikonal methods (Vidale, 1990; van Trier and Symes, 1991; Podvin and Lecomte, 1991; Fomel, 1997) can efficiently produce first arrivals, but in areas of complex geology the first arrival is not always the most important arrival (Audebert et al., 1997). Nichols (1994) proposed a band-limited method that gave the maximum amplitude arrival, but the method is computationally impractical in 3-D. As a result, people usually go to expensive ray based methods but still face the difficult tasks of choosing the most important arrival and correctly and efficiently interpolate the traveltime field (Sava and Biondi, 1997).

The most computationally attractive alternative to Kirchhoff methods is frequency domain downward continuation. Downward continuation has its own weaknesses. Its primary weakness is speed. Downward continuation can not be target oriented, so full volume imaging is required. In addition, frequency domains methods in their purest form can not handle lateral variations in velocity. By migrating with multiple velocities and applying a space domain correction to the wavefield, they can do a fairly good job handling lateral variations (this migration is normally referred to as PSPI, Phase-shift plus interpolation)(Ristow and Ruhl, 1993). Finally, downward continuation focuses the wavefield towards zero offset, making conventional moveout analysis impossible.

We can create CRP gathers where moveout analysis is possible by changing our imaging condition (Clayton and Stolt, 1981; Prucha et al., 1999). Given a wave-field we follow the normal procedure of downward continuing the data and extracting the image at the surface $z = 0$ and zero time. Instead of extracting the image at zero offset, we note that reflection angle θ can be evaluated by the differential equation:

$$\tan\theta = -\frac{\partial z}{\partial x_h} \tag{5}$$

where z is the depth, x_h is half-offset.

The topic of this paper is not migration, but tomography. The tomography method could be applied with either Kirchhoff or PSPI. For us, PSPI proved to be a more attractive choice. A 2-D and 3-D PSPI algorithm was already available, where a Kirchhoff approach would have required the coding of the migration algorithm along with a suitable traveltime computation method.

Characterizing moveout errors

Tomography requires us to provide moveout errors. It is unreasonable to hand pick every reflector at every CRP gather in 2-D and inconceivable in 3-D. As a result, people have tried to find alternate methods to pick moveout errors. Clark et al. (1996) used a neural network approach to pick CRP gathers and many people have suggested seeding-based approaches to pick the gathers. Both approaches describe complicated moveouts, but they suffer from cycle skipping and have problems in areas where the S/N ratio is not very high. An alternative

approach is to characterize the moveout in CRP gathers by a single parameter (Etgen, 1990; Biondi, 1990). A single parameter is a much more robust estimator. It requires less human involvement (less picking and/or QA is necessary) and is less sensitive to signal to noise problems.

At early iterations a single parameter is especially valuable. All that can be resolved at early iterations are gross features. A single parameter can capture these where picking the entire CRP gather is likely to cause the inversion to be overwhelmed small features that are not resolvable at early iterations. When we were close to the correct velocity allowing freedom in moveout behavior is desirable and beneficial.

For the tomography problem we will begin with a migrated image d at a depth z, angle θ, at CRP location x. For estimating the residual moveout in the CRP gathers by calculating semblance s in terms of some curvature parameter γ,

$$s(z,c,x) = \frac{\left[\sum_\theta d(z+\theta\gamma^2,\theta,x)\right]^2}{n(z,x)\sum_{j=0} d(z+\theta\gamma^2,x)^2}, \tag{6}$$

where $n(z,x)$ is the number non-zero samples summed over for each semblance calculation.

For this dataset hand picking the semblance along each reflector would not be too tedious, but in 3-D it would quickly become so. As a result, we wanted to come up with a simple way for the computer to do most of the work. One option would be to just pick the maximum semblance at each location, but we can get an unrealistic, high spatial wavenumber behavior for $\gamma(x)$. When doing convention semblance analysis we are confronted with a similar problem, that picking the maximum semblance at each time could result in an unreasonable velocity function. Clapp et al. (1998b) proposed a method to avoid hand picking that still led to a reasonable velocity model. We can adapt that work by starting with the maximum curvature value at each CRP $\boldsymbol{\gamma}_{\mathbf{max}}$, the semblance at the maximum curvature value $\mathbf{W}$, and a derivative operator $\mathbf{D}$. We can find a smooth curvature function $\boldsymbol{\gamma}$ by setting up a simple set of equations

$$\begin{aligned} \mathbf{0} &\approx \mathbf{W}(\boldsymbol{\gamma}_{\mathbf{max}} - \boldsymbol{\gamma}) \\ \mathbf{0} &\approx \epsilon \mathbf{D}\boldsymbol{\gamma}. \end{aligned} \tag{7}$$

By increasing ϵ we get smoother $\boldsymbol{\gamma}$ values while small ϵ values honor more our maximum semblance picks.

Endpoints, edge effects, and errors

To set up our tomography problem we need to cover some final details. We can convert our semblance picks back into a Δz shift by applying

$$\Delta z = \gamma\theta^2. \tag{8}$$

We then note that our tomography problem is set up for time rather than depth errors, To convert our depth error to a time error we multiplying by RMS slowness s_{rms} of. If we use

a straight ray geometric assumption, we can approximate the time error at a given offset by multiplying by $\cos\theta$ and $\cos\phi$ (where ϕ is the geologic dip) obtaining as our final relationship

$$\Delta t = \frac{2\gamma\theta^2 \cos\theta \cos\phi}{v(z,\mathbf{x})}. \tag{9}$$

In constructing our raypaths we benefit from having our CRP gathers in terms of angle. If errors were in terms of offset we would have to either

- shoot rays from every source and receiver location, and find ray pairs that obey Snell's law at the position on the reflector imaged at the offset dictated by the ray pair
- or shoot rays from our CRP locations along where our reflector is imaged at every offset and then interpolate the ray field to our source and receiver locations.

Both options require significant additional ray-tracing in 2-D, and even more in 3-D. In addition, we are always faced with the tradeoff of how much should we interpolate our rays versus how many additional rays should we shoot.

With our moveout errors in terms of angle we only need to shoot a single ray-pair up from our imaging point at the angle α and β,

$$\begin{aligned} \alpha &= \phi+\theta \\ \alpha &= \phi-\theta \end{aligned} \tag{10}$$

where θ is one-half the aperture angle, ϕ is the geologic dip (Figure 1). If the rays emerge at surface locations corresponding to an offset and CMP location inside our acquisition geometry we have a valid ray pair.

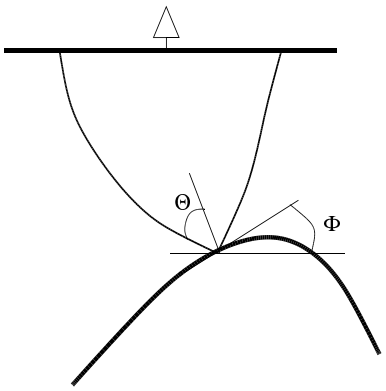

Figure 1: How the takeoff angle for a ray-pair are defined. bob1-sketch [NR]

DATA

The tomography method described in the preceding section is suited for a particular class of problems. Using rays and picking reflectors requires that the dataset it is applied to be

relatively clean with strong, fairly continuous reflectors. Formulating the tomography in tau is universally advantageous, but is most advantageous in environments where we have a velocity inversion. Finally, steering filters are most effective when velocity follows structural dip, ruling out most Gulf of Mexico environments.

The North Sea dataset provided to SEP by Elf Aquitaine (Vaillant and Sava, 1999; Sava and Fomel, 2000; Fomel, 2000) meets all of these criteria. The data is very clean (Figure 2) with strong reflectors that are generally continuous. The data contains a chalk layer which causes a velocity inversion above the salt dome. The initial velocity model (Figure 3) was created by Elf using the S.M.A.R.T[2] method (Jacobs et al., 1992; Ehinger and Lailly, 1995) The velocity structure shows typical North Sea behavior with velocity following structural layers.

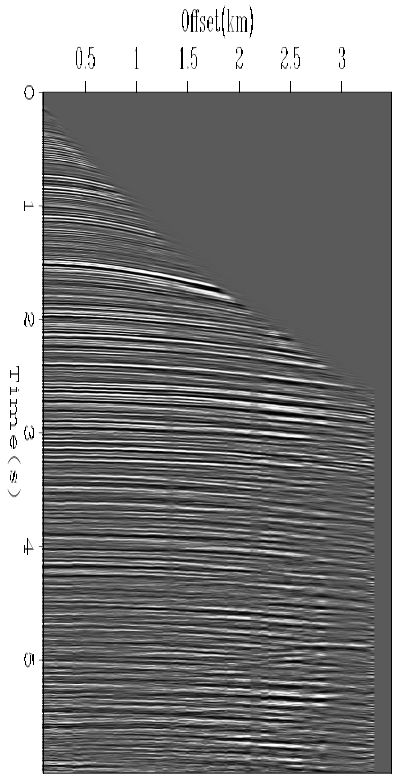

Figure 2: A shot gather from the Elf Aquitaine dataset. bob1-elf-shot [ER]

The dataset is a 3-D marine acquired using three cables with 100 meter spacing and geophones every 25 meters. In this paper we will be dealing with a 2-D subset of the 3-D dataset. The line was chosen coincide with a 2-D synthetic dataset (Prucha et al., 1998; Malcotti and Biondi, 1998). The subset was created by forming partial stacking and then applying Azimuth Moveout (AMO) (Biondi et al., 1998a) to partial stacked CMP gathers.

[2]Sequential Migration-Aided Reflection Tomography - KIM (Kinematic Inversion Methods), IFP consortium

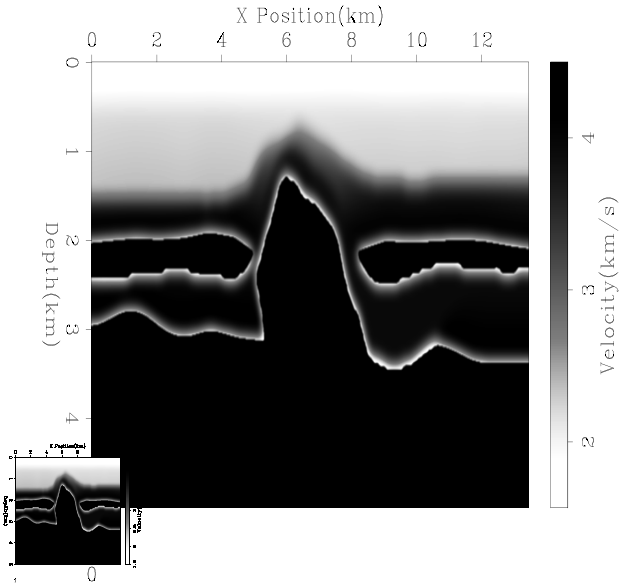

Figure 3: The initial velocity model for the 2-D line. Note how velocity follows structural dip and the velocity reversal in the shale layer above the salt dome. bob1-elf.vel0 [ER]

INITIAL ERRORS

We began by migrating the data with the velocity in Figure 3. As Figure 4 shows we have some artifacts in the right portion of the migrated image due to the sharp boundary in the initial velocity model. The salt is poorly defined. We don't have a coherent reflection for the top of the salt, we have very little of the salt edges, and have a non-continuous salt bottom. Reflections to the left of the salt body do not continue all the way to the salt edge. In addition, we have little resolution below the fault at 10 km. If we look at the angle gathers for the initial migration, Figure 5, we can see significant moveout errors. Using the initial migrated image we chose 11 reflectors to perform tomography with (Figure 6). To constrain the upper portion of the model we chose the water bottom reflection and two reflectors above the salt. We picked the salt top and salt bottom and three reflectors on both sides of the salt body. We then performed moveout analysis using equation (6). We selected the semblance at each reflector, Figure 7, and found a smooth curve using fitting goals (9). Overlaid on Figure 7 are the smooth picks used in our back projection operator. The top two reflectors have have almost no moveout errors. The remaining reflectors all have some residual moveout errors that our tomography can attempt to resolve.

Building the steering filters

To construct the steering filters we used the nine non-salt reflectors shown in Figure 6. We calculated the dip along each reflector and then smoothly interpolated between the reflectors (Figure 8). With the picked reflectors we have very few rays passing through the salt. As a result the smoothing fitting goal (the second goal in (4)) dominates. Instead of constant or little variation in the salt we see dramatic changes. To avoid this geologically unreasonable behavior we did not allow the velocity to change in the region delineated by our two salt reflectors.

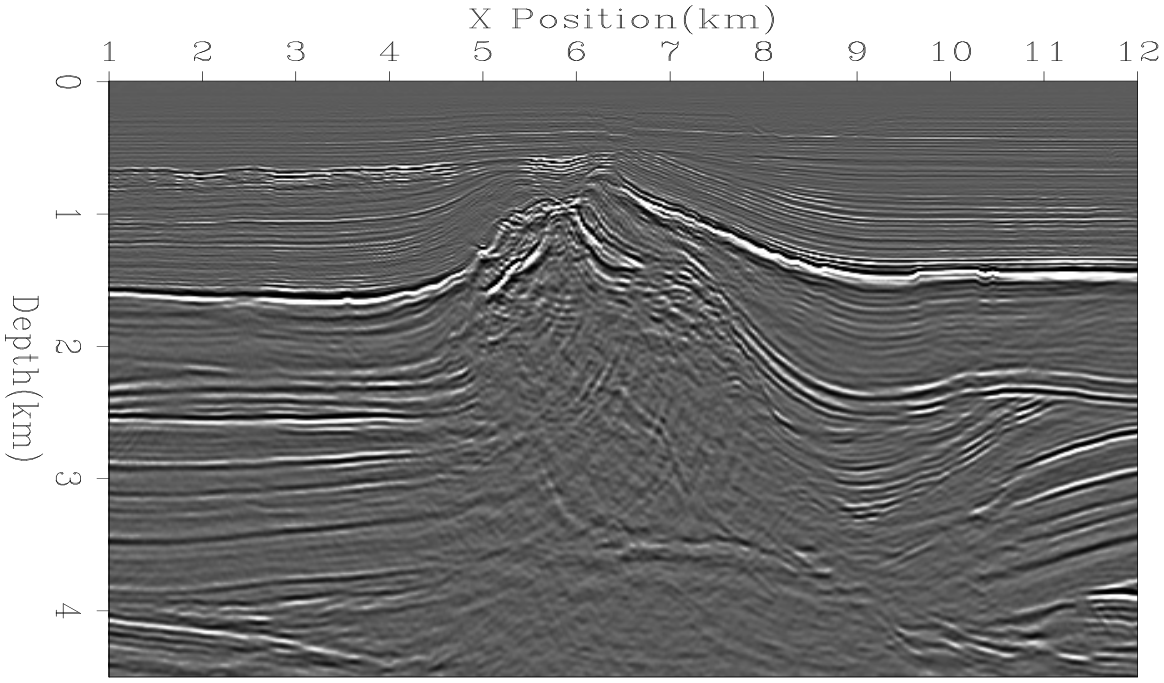

Figure 4: Migration result using the velocity from Figure 3 bob1-elf.mig.vel0 [CR]

RESULTS

We performed two non-linear iteration of tomography. Figure 9 shows our velocity model. Note that our velocity still follows structural dip. This is especially obvious around the fault at 10 km and above the top of the salt. If we examine the same CRP gathers, Figure 11, we see that we have done a better job flattening the reflectors and have higher frequency events. If we look at the semblance along the reflectors, Figure 10, we see that have significantly less moveout. The true test is the final migrated image. If we look at the final migrated image we can see better continuity of the reflectors and generally higher frequency image. The final migration image (Figure 12) is quite similar to our initial image (Figure 4). If we take a closer look at the top of the salt body (Figure 13) we can begin to see some differences. At location 'A' and 'C' we have done a better job defining the salt boundary. At 'B' the reflector is sharper and has a more realistic shape. If we look at the side of the saltdome, Figure 14, we can see more improvements. The reflectors are more continuous 'A' and extend closer to the salt boundary 'B'. We also have done a better job recovering the bottom salt reflector, 'C'.

CONCLUSIONS

In this paper we applied our tomography methodology to a 2-D dataset. We showed how to construct a complex steering filter operator based on reflector geometry and *a priori* knowledge of the acoustic properties of the layers. The final migration result was significantly improved over the initial migration showing flatter angle gathers and overall crisper image.

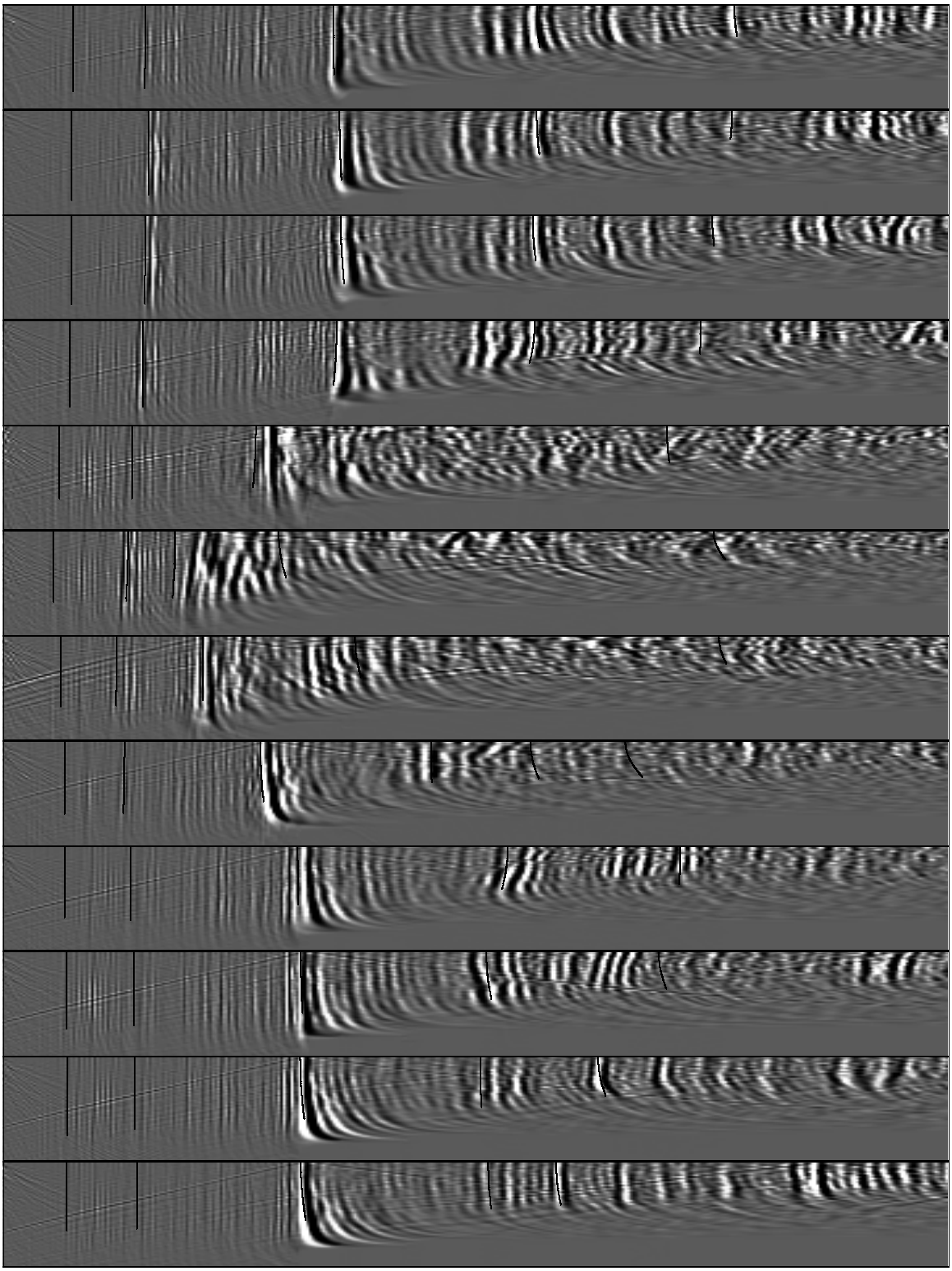

Figure 5: CRP gathers from the initial velocity overlaid by the moveout picks for the reflectors used in the first iteration of tomography. bob1-overlays.vel0 [CR]

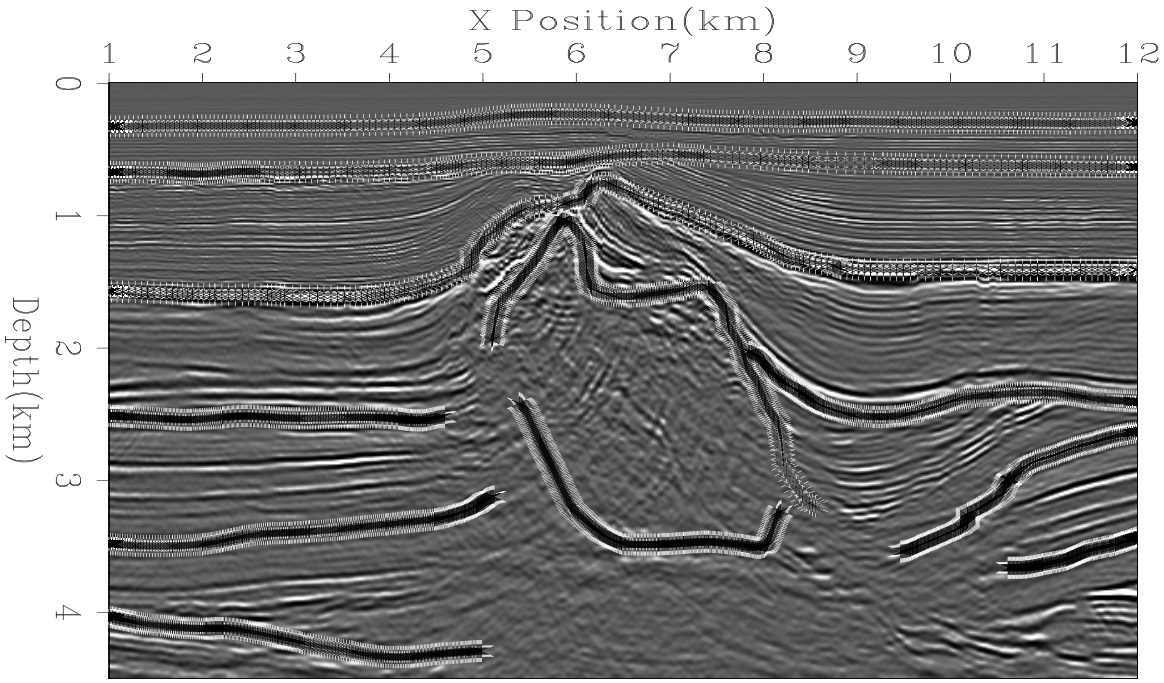

Figure 6: Initial migration with picked reflectors overlaid. bob1-overlays [CR]

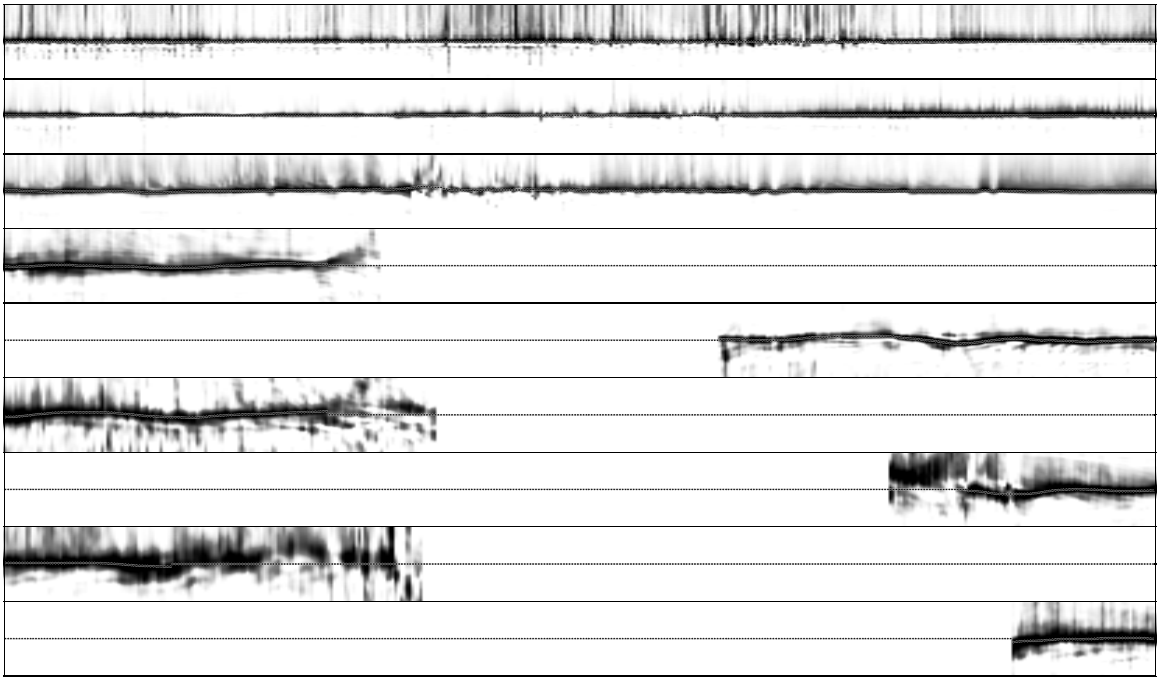

Figure 7: Semblance panels from nine of the reflectors used in tomography. Note that all but the top two still have significant residual moveout. bob1-elf-semb-mig0-ref [CR]

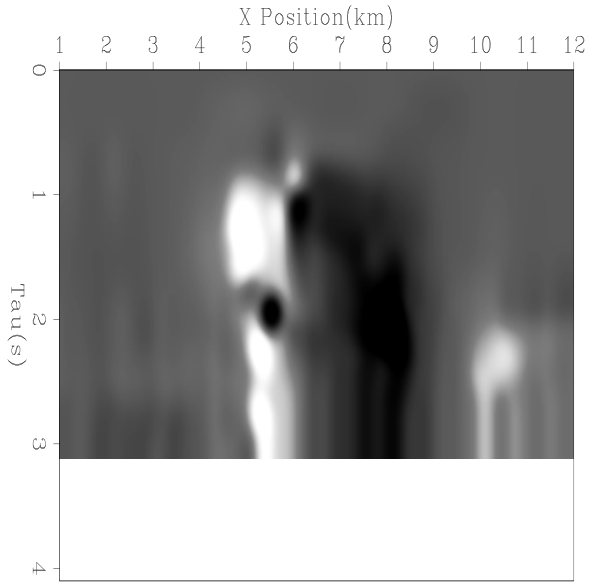

Figure 8: The dip field used for the first iteration of tomography. bob1-amp-vel0 [ER]

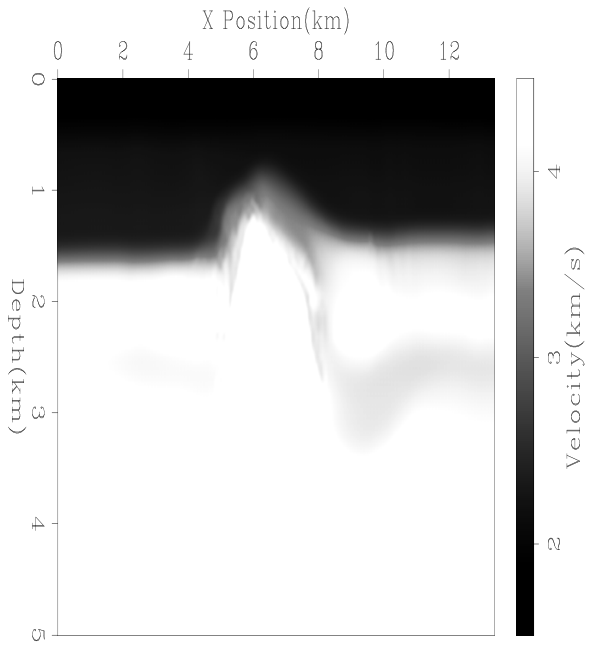

Figure 9: Final velocity bob1-vel-final [CR]

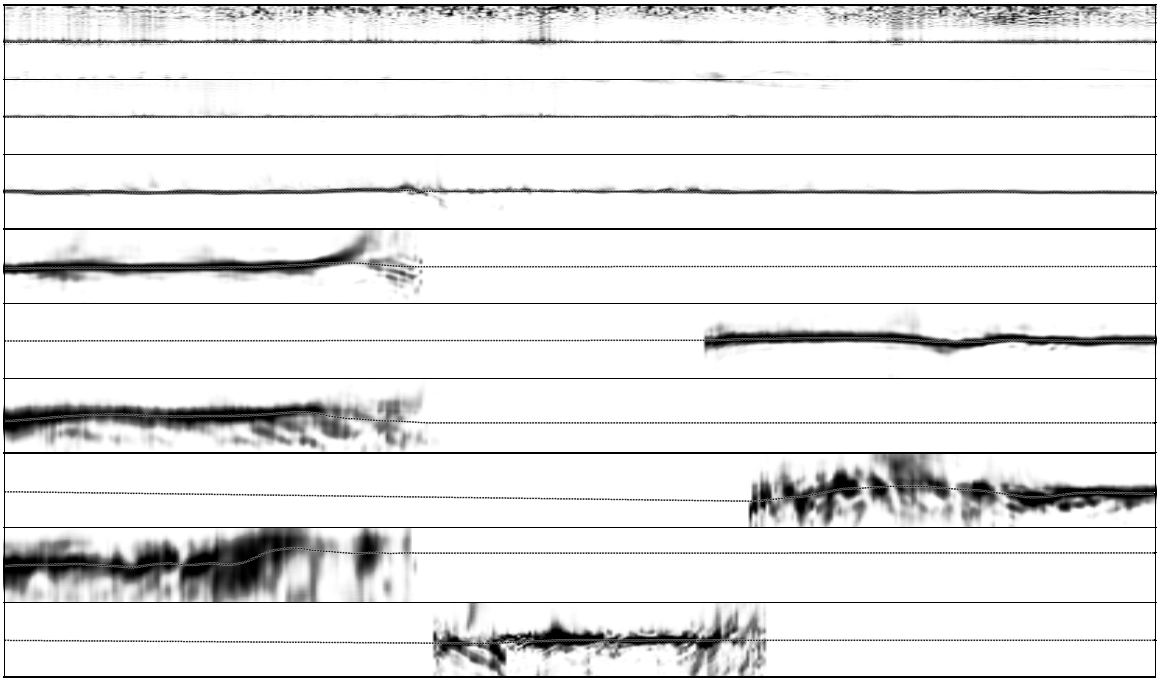

Figure 10: Semblance along the reflectors using final velocity model. bob1-elf-semb-mig-final-ref [CR]

We hypothesize that much of the remaining moveout is due to 3-D effects, not resolvable by a 2-D algorithm.

ACKNOWLEDGEMENTS

We would like to thank Elf for providing the data.

REFERENCES

Al-Chalabi, M., 1997, Parameter nonuniqueness in velocity versus depth functions: Geophysics, **62**, no. 03, 970–979.

Audebert, F., Nichols, D., Rekdal, T., Biondi, B., Lumley, D. E., and Urdaneta, H., 1997, Imaging complex geologic structure with single-arrival kirchhoff prestack depth migration: Geophysics, **62**, no. 05, 1533–1543.

Biondi, B., Fomel, S., and Chemingui, N., 1998a, Azimuth moveout for 3-d prestack imaging: Geophysics, **63**, no. 02, 574–588.

Biondi, B. L., Clapp, R. G., Fomel, S. B., and Alkhalifah, T. A., 1998b, Robust reflection tomography in the time domain: 68th Annual Internat. Mtg., Soc. Expl. Geophys., Expanded Abstracts, 1847–1850.

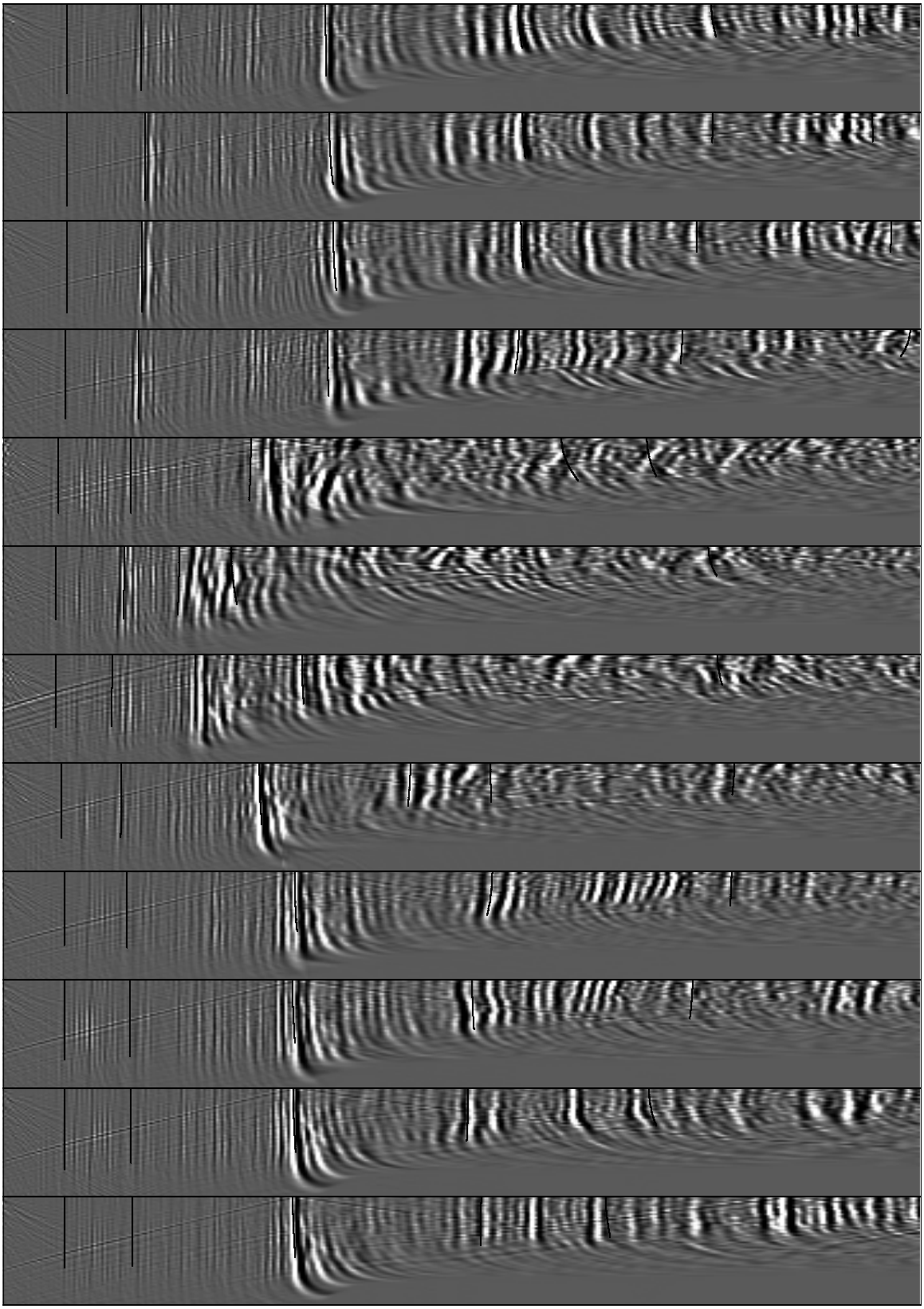

Figure 11: CRP gathers after final migration. bob1-overlays.vel-final [CR]

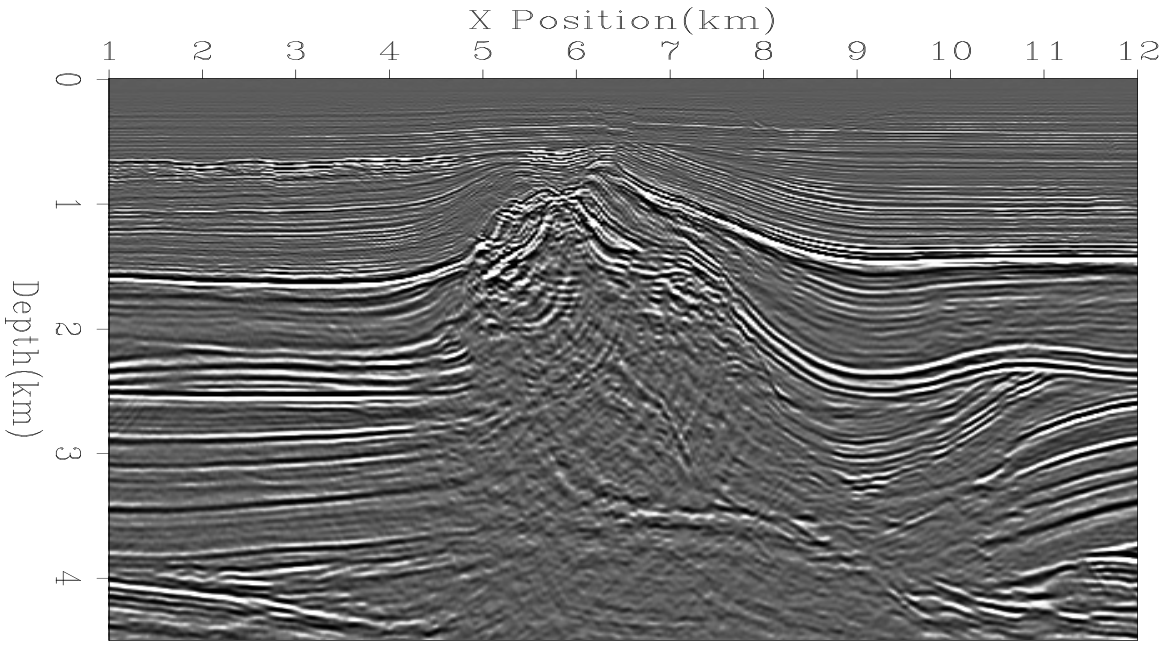

Figure 12: Final migrated image. bob1-mig-final [CR]

Biondi, B., 1990, Velocity analysis using beam stacks: Ph.D. thesis, Stanford University.

Clapp, R. G., and Biondi, B., 1999, Preconditioning tau tomography with geologic constraints: SEP–**100**, 35–50.

Clapp, R. G., Biondi, B. L., Fomel, S. B., and Claerbout, J. F., 1998a, Regularizing velocity estimation using geologic dip information: 68th Annual Internat. Mtg., Soc. Expl. Geophys., Expanded Abstracts, 1851–1854.

Clapp, R. G., Sava, P., and Claerbout, J. F., 1998b, Interval velocity estimation with a null-space: SEP–**97**, 147–156.

Clark, G. A., Glinsky, M. E., Devi, K. R. S., Robinson, J. H., Cheng, P. K. Z., and Ford, G. E., 1996, Automatic event picking in pre-stack migrated gathers using a probabilistic neural network: 66th Annual Internat. Mtg., Soc. Expl. Geophys., Expanded Abstracts, 735–738.

Clayton, R. W., and Stolt, R. H., 1981, A born-wkbj inversion method for acoustic reflection data: Geophysics, **46**, no. 11, 1559–1567.

Ehinger, A., and Lailly, P., 1995, Velocity model determination by the SMART method, part 1: Theory: 65th Annual Internat. Mtg., Soc. Expl. Geophys., Expanded Abstracts, 739–742.

Etgen, J., 1990, Residual prestack migration and interval velocity estimation: Ph.D. thesis, Stanford University.

Fomel, S., Clapp, R., and Claerbout, J., 1997, Missing data interpolation by recursive filter preconditioning: SEP–**95**, 15–25.

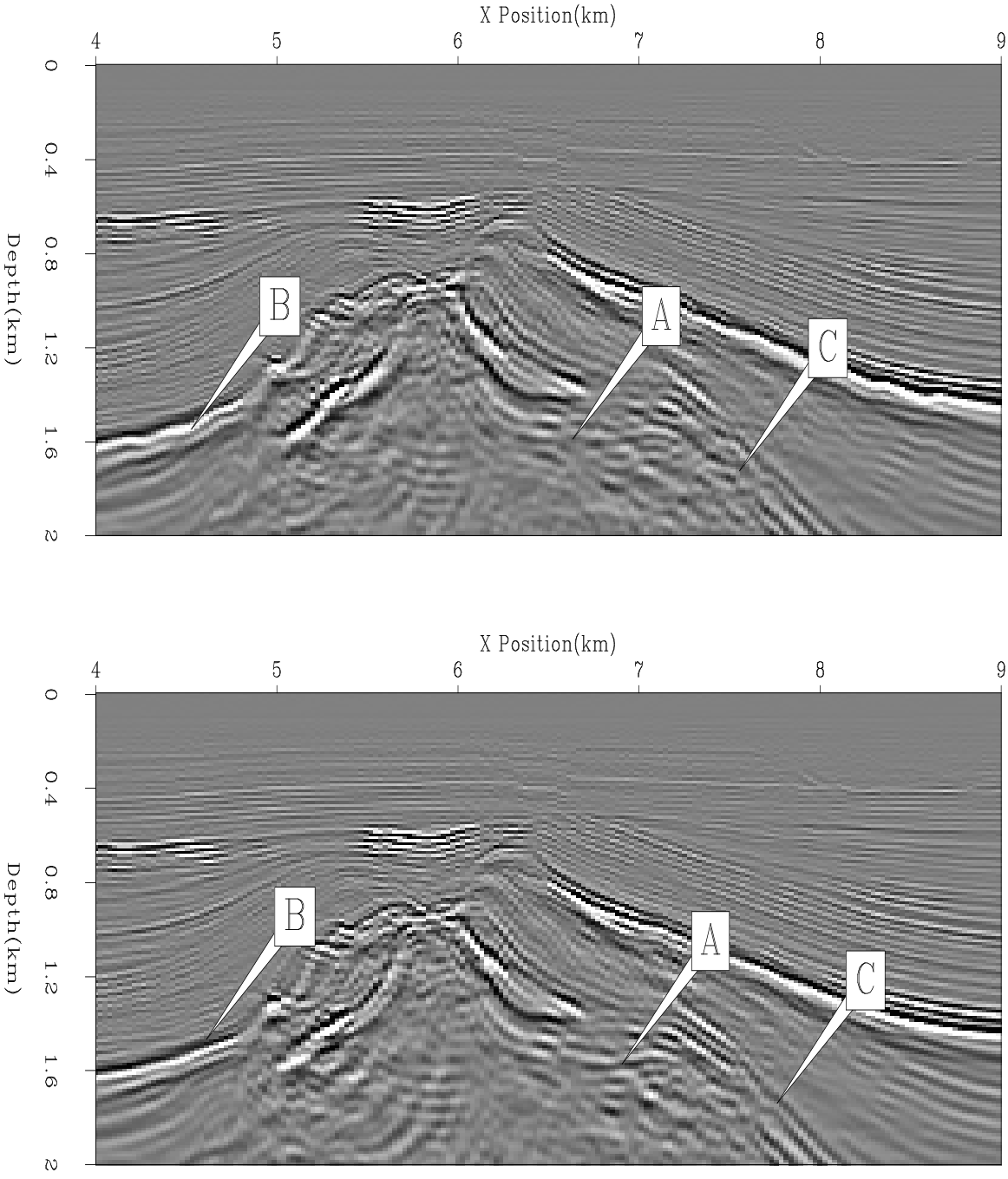

Figure 13: Comparison at the top of the salt dome. At location ‘A’ and ‘C’ we have done a better job defining the salt boundary. At ‘B’ we can see that the reflector is sharper and has a more realistic shape. bob1-mig-top [CR]

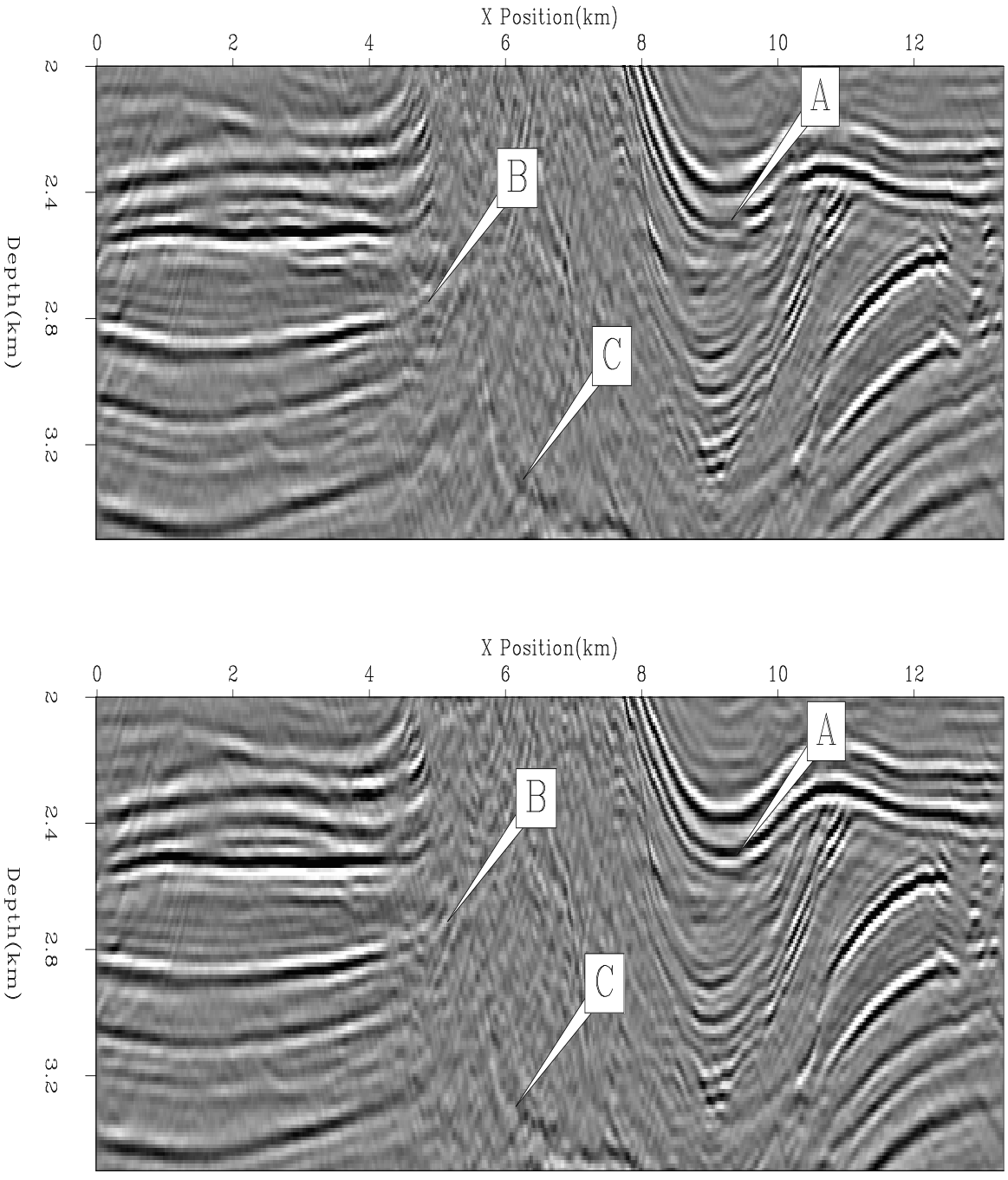

Figure 14: Comparison of the top of the salt dome. The reflectors are more continuous ‘A’ and extend closer to the salt boundary ‘B’. We also have done a better job recovering the bottom salt reflector, ‘C’. bob1-mig-side [CR]

Fomel, S., 1997, A variational formulation of the fast marching eikonal solver: SEP–**95**, 127–147.

Fomel, S., 2000, Helical preconditioning and splines in tension: SEP–**103**, 289–301.

Jacobs, J. A. C., Delprat-Jannaud, F., Ehinger, A., and Lailly, P., 1992, Sequential migration-aided reflection tomography: A tool for imaging complex structures: 62nd Annual Internat. Mtg., Soc. Expl. Geophys., Expanded Abstracts, 1054–1057.

Malcotti, H., and Biondi, B., 1998, Accurate linear interpolation in the extended split-step migration: SEP–**97**, 61–72.

Nichols, D. E., 1994, Imaging complex structures using band-limited Green's functions: SEP–**81**.

Podvin, P., and Lecomte, I., 1991, Finite difference computation of traveltimes in very contrasted velocity models: A massively parallel approach and its associated tools: Geophysical Journal International, **105**, 271–284.

Prucha, M. L., Clapp, R. G., and Biondi, B. L., 1998, Imaging under the edges of salt bodies: Analysis of an Elf North Sea dataset: SEP–**97**, 35–44.

Prucha, M. L., Biondi, B. L., and Symes, W. W., 1999, Angle-domain common image gathers by wave-equation migration: 69th Annual Internat. Mtg., Soc. Expl. Geophys., Expanded Abstracts, 824–827.

Ristow, D., and Ruhl, T., 1993, Extended split-step migration by cascading phase shift and finite difference operators: 63rd Annual Internat. Mtg., Soc. Expl. Geophys., Expanding Abstracts, 986–989.

Sava, P., and Biondi, B., 1997, Multivalued traveltime interpolation: SEP–**95**, 115–126.

Sava, P., and Fomel, S., 2000, Angle-gathers by Fourier Transform: SEP–**103**, 119–130.

Stork, C., and Clayton, R. W., 1991, An implementation of tomographic velocity analysis: Geophysics, **56**, no. 04, 483–495.

Tarantola, A., 1987, Inverse problem theory: Elsevier.

Tieman, H. J., 1995, Migration velocity analysis: Accounting for the effects of lateral velocity variations: Geophysics, **60**, no. 01, 164–175.

Toldi, J., 1985, Velocity analysis without picking: SEP–**43**.

Vaillant, L., and Sava, P., 1999, Common-azimuth migration of a North Sea dataset: SEP–**102**, 1–14.

van Trier, J., and Symes, W. W., 1991, Upwind finite-difference calculation of traveltimes: Geophysics, **56**, no. 6, 812–821.

van Trier, J., 1990, Tomographic determination of structural velocities from depth migrated seismic data: Ph.D. thesis, Stanford University.

Vidale, J. E., 1990, Finite-difference calculation of traveltimes in three dimensions: Geophysics, **55**, no. 5, 521–526.